Journal of Civil Structural Health Monitoring
https://doi.org/10.1007/s13349-020-00387-3

ORIGINAL PAPER

Long-term strain measurements of traffic and temperature effects on an RC bridge deck slab strengthened with an R-UHPFRC layer

Bartłomiej Sawicki[1] · **Eugen Brühwiler**[1]

Received: 22 October 2019 / Revised: 12 February 2020 / Accepted: 13 February 2020

Abstract
This paper presents the results of 28-month-long monitoring of a slab portion of the Chillon viaducts in Switzerland using strain gauges and thermocouples. This post-tensioned reinforced concrete structure was strengthened with a layer of reinforced ultrahigh-performance fibre-reinforced cementitious composite (UHPFRC). The strain gauges are used to measure stresses in the bottom layer of reinforcement bars in the slab, while thermocouples explain the behaviour of the structure due to temperature variation. The response under both traffic and thermal actions is discussed. It is demonstrated that the stress variation due to the thermal action can be as large as the response due to traffic action even in such a massive structure. Furthermore, recommendations for analysing both traffic and thermal-induced stresses are given. The commonly used simplified method for calculation of fatigue stress is shown to be highly conservative, leading to overestimation of structural action effects by a factor of four.

Keywords Strain measurements · Monitoring · UHPFRC · Fatigue · Bridges

1 Introduction

The examination of bridges under service conditions is challenging because of multiple actions applied to the structure, such as repetitive loads and temperature variation. Regarding fatigue safety verification, virtually any existing bridge recalculated using current standards fails [1]. This is why monitoring and understanding of the real action effects on bridge elements is important, especially regarding the fatigue.

The Chillon viaducts, in service since 1969, are two parallel structures with a total length of 2.1 km each and spans varying from 92 to 104 m. This post-tensioned concrete structure was strengthened in 2014/2015 by a layer of reinforced ultrahigh-performance fibre-reinforced cementitious composite (R-UHPFRC) cast on top of the deck slab, since structural and fatigue safety was of concern. The layer of UHPFRC accommodating steel reinforcement bars was casted to increase the stiffness and structural resistance of the deck slab and the box girder, and to serve as a waterproofing layer protecting the existing reinforced concrete [2]. A monitoring campaign was commenced in May 2016 to verify the effectiveness of the UHPFRC-strengthening [3]. This method of rehabilitation and strengthening of reinforced concrete bridges has been developed over the last 20 years [4], became an established technique in Switzerland [5, 6] and is now emerging in other countries.

The direct measurement of traffic action effects is a reliable and cost-efficient method of quantification of structural demand. The collected data can be used to verify the safety of existing structures [7, 8]. This approach is applicable for fatigue verification of bridges [9, 10] where the effects of repeating actions are of importance. Additionally, thanks to direct monitoring, the behaviour under traffic and temperature actions can be analysed leading to better understanding of how the bridge works on the structural level, and to verify the prior assumptions [11, 12].

Numerous monitoring campaigns have led to reduction of uncertainties in structural demand and thus more reliable safety verification. For example, Sousa et al. [11] performed long-term strain monitoring of traffic action effects on the box girder of the Leziria Bridge. The strain gauges

✉ Bartłomiej Sawicki
bartek.sawicki@epfl.ch

Eugen Brühwiler
eugen.bruehwiler@epfl.ch

[1] Laboratory for Maintenance and Safety of Structures, Civil Engineering Institute, Swiss Federal Institute of Technology Lausanne (EPFL), Lausanne, Switzerland

Published online: 03 March 2020

were compensated for the temperature expansion, but the measured temperature-induced strains were neglected. A similar approach was followed by Treacy and Brühwiler [13] in the monitoring of two box girder highway viaducts. Massicotte and Picard [14] performed extensive monitoring campaign of the massive box girder of the Grand-Mere Bridge using strain gauges and thermocouples. On the basis of measured temperature gradients, they built a finite element model to assess the thermally induced stresses. However, no verification using strain gauges was done. Chen et al. [15] combined strain and temperature monitoring to quantify temperature-induced stresses. Results were further analysed together with acceleration measurements to calculate the reliability of the structure. No long-term dynamic strain measurements were done.

Literature review shows that the contribution of thermally induced stress range to the fatigue damage is disregarded in most monitoring campaigns, albeit it might be significant [12]. Researchers are rather interested in the extreme values of temperature gradient, which is important as well [16]. The objective of this paper is to quantify the structural response of the bridge deck under combined traffic and thermal actions. The quick and computationally efficient method of data analysis from the point of view of fatigue limit state is presented. The relevance of thermally induced stress cycles is discussed as well.

2 Description of the monitoring system

The monitoring system presented in this paper is composed of four strain gauges and eight thermocouples. Since the fatigue resistance of reinforced concrete is governed by the steel reinforcing bars [17–20], the bottom layer of rebars of the deck slab is instrumented.

The strain gauges are glued in two locations (Fig. 1). Group 1 is located at mid span, on the central axis of the slab, where the longitudinal and transversal bars cross. Group 2 is placed at a distance of around 50 cm from the first one, again at a crossing point of rebars. At each of the two locations, one gauge is glued, respectively, on the longitudinal and transversal rebars. To do so, the rebars were detected and then the cover concrete was carefully removed to expose the reinforcement.

The seven thermocouples are glued on the concrete surface along the perimeter of the box girder, inside. Additionally, the air temperature in the box girder is recorded.

The signals from the strain gauges are recorded with a frequency of 100 Hz, and from thermocouples with a frequency of 1 Hz. The frequency is chosen to get the minimum file size while not losing any important strain peak due to the traffic. Still, about 200 MB of data are collected daily. The present paper exploits the data collected between January 20, 2017 and April 10, 2019. Due to technical problems, some days of recording were omitted resulting in 602 full days of monitoring data.

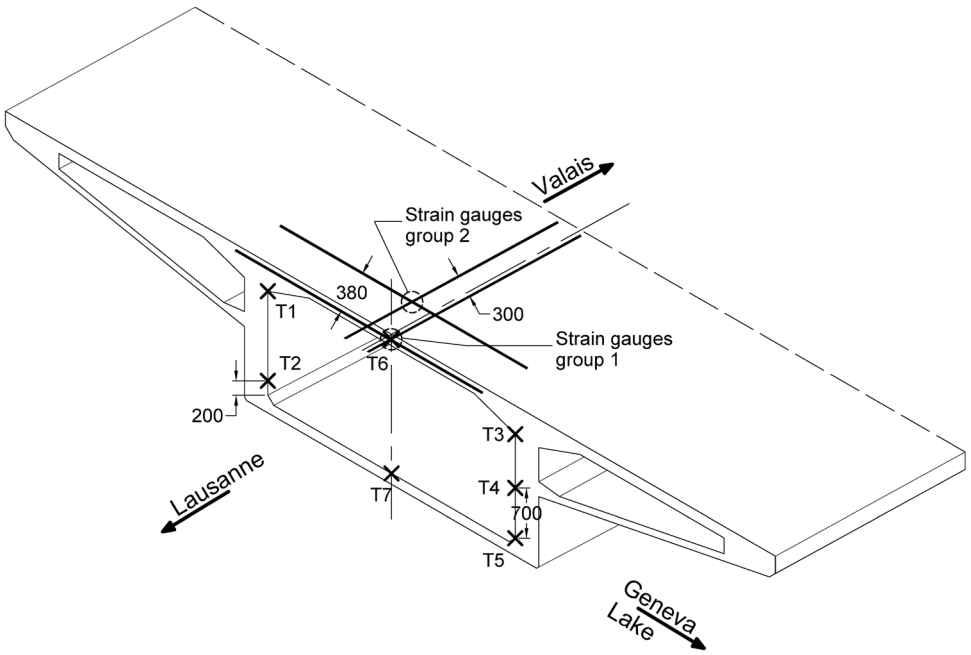

Fig. 1 Scheme of monitoring; T1–T7: thermocouples; dimensions in mm

3 Structural response due to single traffic events

The signal recorded with the data acquisition system (DAQ) is composed of the traffic-induced strain ranges and the "thermal wave", as presented in Fig. 2. To analyse the monitoring results, the two kinds of signals are separated. Since the variation of strains due to the "thermal wave" is much slower than traffic-induced strains, a running average function is used. The signal resulting from this operation presents only the thermal response of the structure. If this signal is subtracted from the original one, only the structural response due to the traffic action is obtained [13]. In this paper, the consequences of this separation are discussed.

The structural behaviour of the deck slab under traffic loading is discussed here on the basis of single truck passages for the sake of clarity. Figure 3 presents the strain signals recorded by the four strain gauges at the same instance of time, and the truck that could possibly produce this response. Since there is no visual monitoring of the vehicles on the viaduct, the type of truck cannot be determined precisely.

The transversal rebar response is exclusively local, and it is subjected to the tensile cycles due to the passage of each axle. The response of rebars in the longitudinal direction depends on the weight of the passing truck. In the case of a normal 5-axle truck of 40 t of weight or a 50 t crane, the global box girder response produces compressive stresses in the slab. Thus, in addition to compressive stress, the longitudinal rebar is subjected to tensile local stress under the wheel load, leading to the tensile–compressive reversal stress cycles. However, for an extremely heavy special transport using multi-axle lowboy truck, the global behaviour is so pronounced that there is no tensile stress in the rebar. The response due to each axle is still visible, but the strain is always negative leading to one pronounced compressive cycle rather than multiple tensile cycles. Thanks to the almost equal load distribution among axles, the recorded transversal strains are comparable with the ones from the 40 t truck.

The transversal rebar is more sensitive than the longitudinal one to the position of truck on the traffic lane. The strain differences recorded by the two transversal gauges are much larger than the strain differences obtained from the longitudinal rebars for 40 t and lowboy trucks. However, for the 50 t crane these differences are much smaller, probably because the crane was travelling very close to the fast lane or even on the fast lane.

Overall, the transversal rebar shows only local response due to axle passage, while the longitudinal bars present a mixture of global and local response under traffic loading. Importantly, the fatigue-relevant damage is not directly linked to the truck or axle load, which shows the importance of direct strain and stress measurements in existing bridges to obtain realistic data for fatigue safety verification.

4 Structural response due to temperature variation

4.1 Diurnal variation of temperature

The monitored part of the viaduct is oriented approximately along the north–south direction. From the east, it

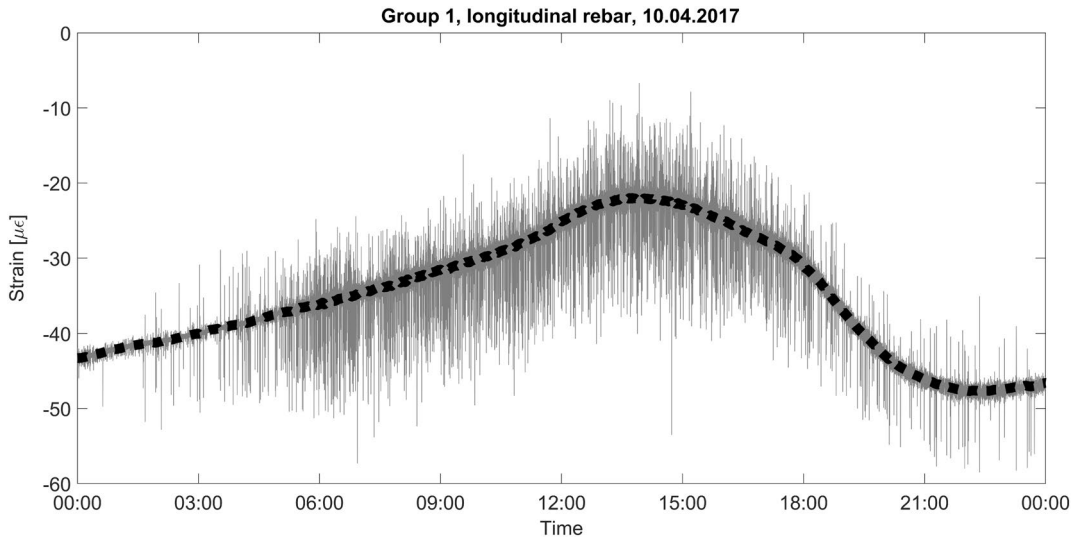

Fig. 2 Strain recorded during 1 day on longitudinal rebar, Group 1; filtered-out "thermal wave" shown with dotted line

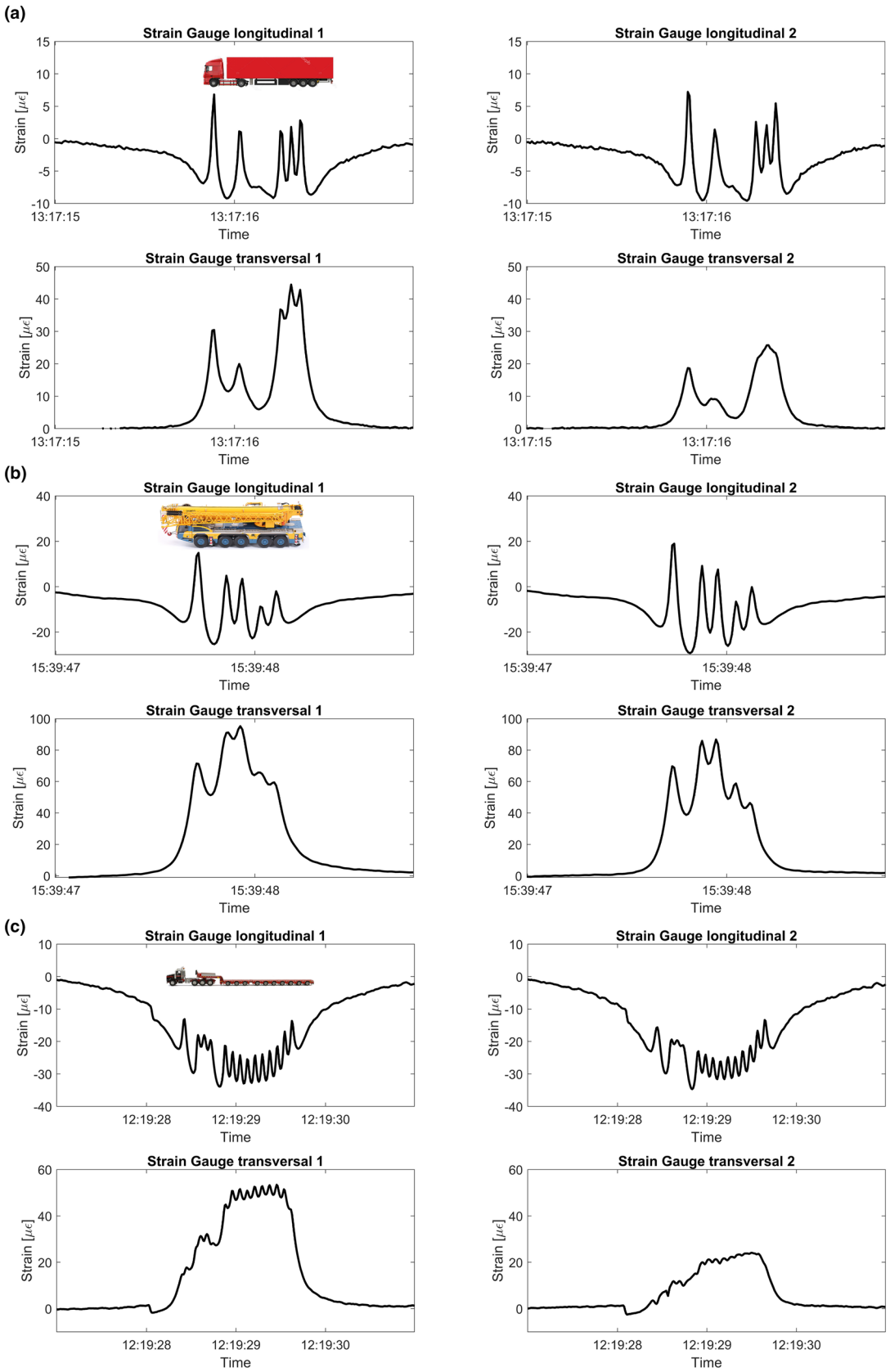

Fig. 3 **a** Typical five axle truck, recorded on 10.04.2017; **b** five axle mobile crane, recorded on 23.06.2017; **c** exceptionally long lowboy truck, recorded on 15.03.2018

is close to the slope of a mountain and the neighbouring viaduct, while the western part is fully exposed due to the situation next to the lake. The effect of this orientation will be discussed below using the example of a randomly chosen day (10.04.2017). Due to its situation, the structure remains shadowed in the morning, while being exposed to the sun in the afternoon until the sun sets. Since the temperature is measured on the bottom face of the concrete slab and in the box girder, additional delay due to the heat transfer across the slab is observed. Thus, the lowest recorded temperature occurs at around noon (Fig. 4).

The largest temperature variation is recorded by thermocouples T6 and T7, which are located, respectively, on the upper and lower slab of the box girder. This is explained by the difference in concrete thickness, i.e. the upper slab thickness is 22 cm and the lower slab is 16 cm, while the webs are 40 cm thick. Additionally, the voids of the cantilever slabs act as thermal insulators. Due to that, the web temperature starts rising approximately 2 h later than the temperature of the slabs.

Within the thermocouples on the webs, the highest temperature is recorded by thermocouples T5, then T4 and T3 respectively. This is explained by the exposition of this wall to the west, where the sun may operate approximately from 3 p.m. until sunset (8 p.m.) on the discussed day (April 10).

The most stable temperature is the one recorded inside of the box girder and is also lower than the temperature of the webs. This depends on the external air temperature during the couple of previous days and is expected [13].

4.2 Strain variation due to temperature

The thermal strain recorded during 1 day is presented in Fig. 5. For the longitudinal strain gauges, the strain is approximately linearly dependent on the temperature of the deck slab. This indicates the expansion along the axis of the viaduct and no loss of stiffness. In case of the transversal gauges, the strain readings form a loop. This is caused by the previously described complex distribution of temperature on the perimeter of the box girder.

4.3 Verification of reliability of results using thermal strains

Figure 6 presents the daily temperature variation and the daily "thermal wave" variation for the whole duration of monitoring. Obviously, the bigger the temperature variation, the bigger are the induced strains. This dependency can be used to verify the reliability of the sensors [21]. The longitudinal gauge of Group 1 followed the thermal amplitude only until spring 2018 when this gauge no longer functioned properly, probably because of humidity due to improper sealing. From this incident on, the data from this gauge are not taken into account. The transversal gauge from Group 2 followed the temperature variation until it failed completely in July 2018. The two other gauges closely followed the temperature variation without inconsistencies during the whole duration of measurement.

4.4 Importance of temperature effects

As mentioned previously, the recorded raw signal is composed of the strain from two sources: thermal and traffic

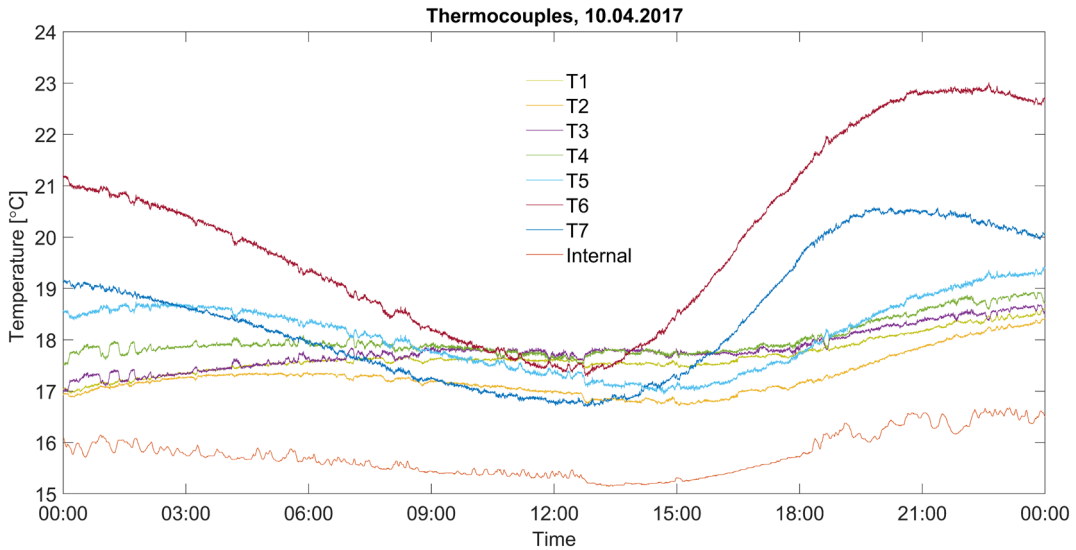

Fig. 4 Temperature recorded during 1 day with all thermocouples

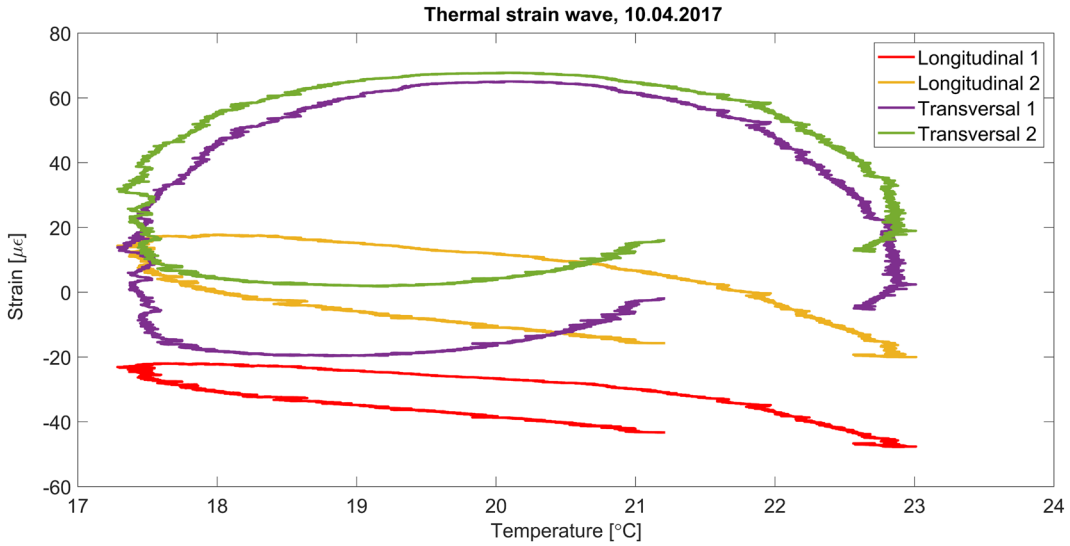

Fig. 5 "Thermal wave" strain vs. temperature recorded on 10.04.2017

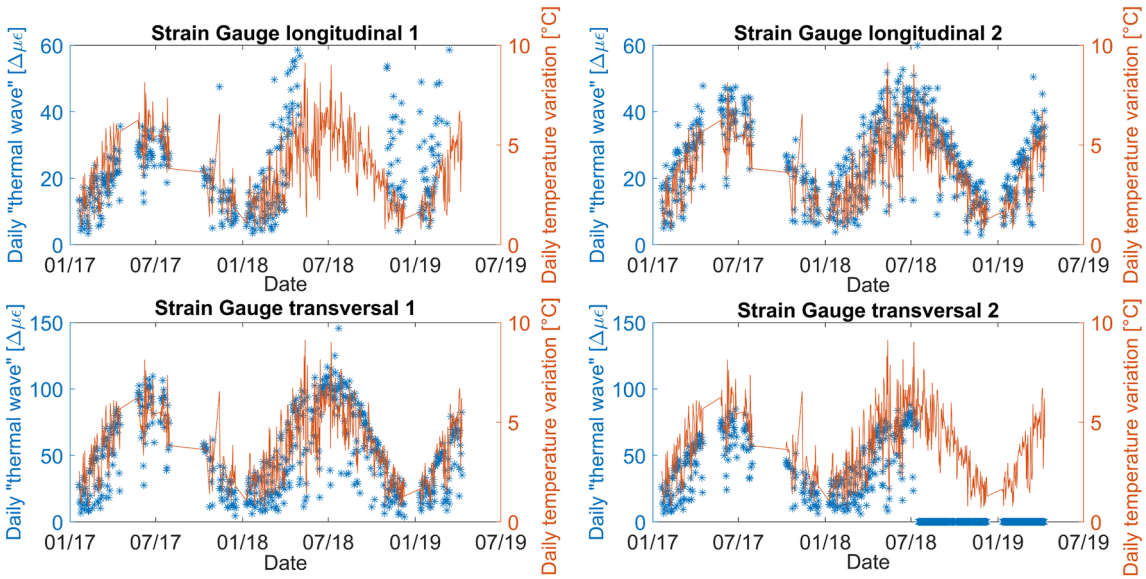

Fig. 6 Daily temperature amplitude and thermal strain variation for the whole monitoring period

actions. When only the vehicle traffic loading is of interest, the thermally induced strains need to be removed. However, with proper instrumentation, the thermal strain readings can carry relevant information as well. In this monitoring campaign, the Poisson half-bridge system was installed, which is a type of the Wheatstone bridge circuit [22]. It is composed of two active gauges, measuring the strain perpendicularly in relation one to another (Fig. 7).

The gauge oriented along the rebar axis measures both the thermal expansion of the slab and the deformations due to the traffic action. Since the concrete cover of the rebar is locally removed, the section of interest is free to expand in the direction perpendicular to bar axis. Thus, the perpendicular gauge records only the free thermal expansion of steel and the strain variation due to Poisson's effect. Thanks to the half-bridge connection, the signal recorded by the perpendicular gauge is subtracted from the signal recorded by the longitudinal gauge, taking into account the Poisson's effect.

The DAQ automatically cancels out the variation of electrical conductivity of cables and measurement unit due to the changes of temperature. Thus, the only source of this difference originates from the strain gauges.

The upper portion of Fig. 7a represents the situation of the gauge that is perpendicular to the rebar axis. If the

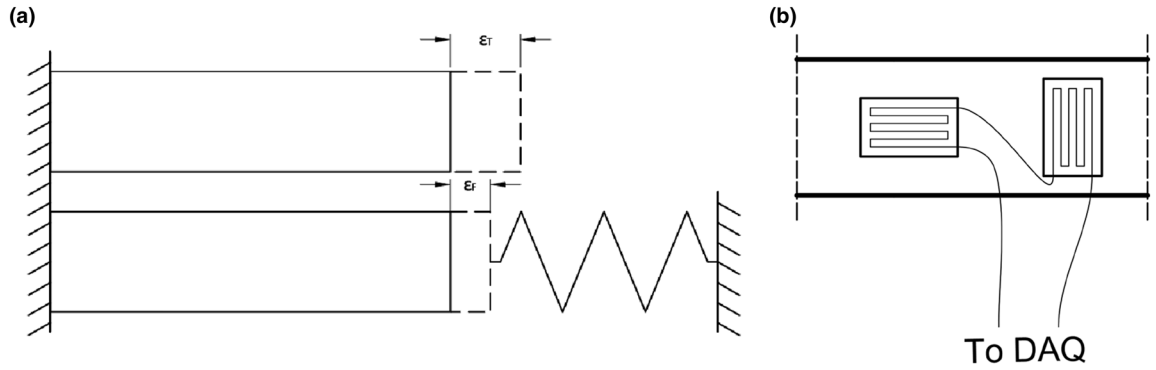

Fig. 7 **a** Free and partially restrained thermal expansion; **b** scheme of strain gauges glued on rebar in half-bridge

Poisson's effect is disregarded, it measures only the free body expansion according to the formula (1):

$$\varepsilon_T = \alpha_T \cdot \Delta T, \tag{1}$$

where ε_T is a free thermal expansion, α_T is the coefficient of thermal expansion and ΔT is the temperature variation.

The measurements taken by the gauge parallel to the rebar's axis are affected due to the partial restraint of the slab that still allows for some free expansion, noted with ε_F. The effect of Wheatstone half-bridge can be described by the relation:

$$\varepsilon_F - \varepsilon_T = -\frac{\sigma_T}{E}, \tag{2}$$

where σ_T is the stress due to partially restrained thermal expansion and E is the modulus of elasticity of steel. The right part of Eq. (2) is recorded by the DAQ as a "thermal wave" as shown by the dotted curve in Fig. 2. Thus, the monitoring system allows for an indirect measurement of the residual thermal stress variation in the structure.

The variation of the residual thermal stresses in the longitudinal and transversal rebars is presented in Fig. 8. In the longitudinal rebar, the structural response is delayed by 1.5 h with respect to the deck slab temperature. The transversal rebar stresses are further delayed, in total by 4 h. The stress variation in longitudinal rebar is mostly dependent on the temperature of the deck slab, while the transversal rebar responses depend on the temperature distribution along the whole box girder perimeter. These effects are common and expected in reinforced concrete structures [12, 13]. Importantly, the stress ranges in the transversal rebar are much larger than that in the longitudinal rebar.

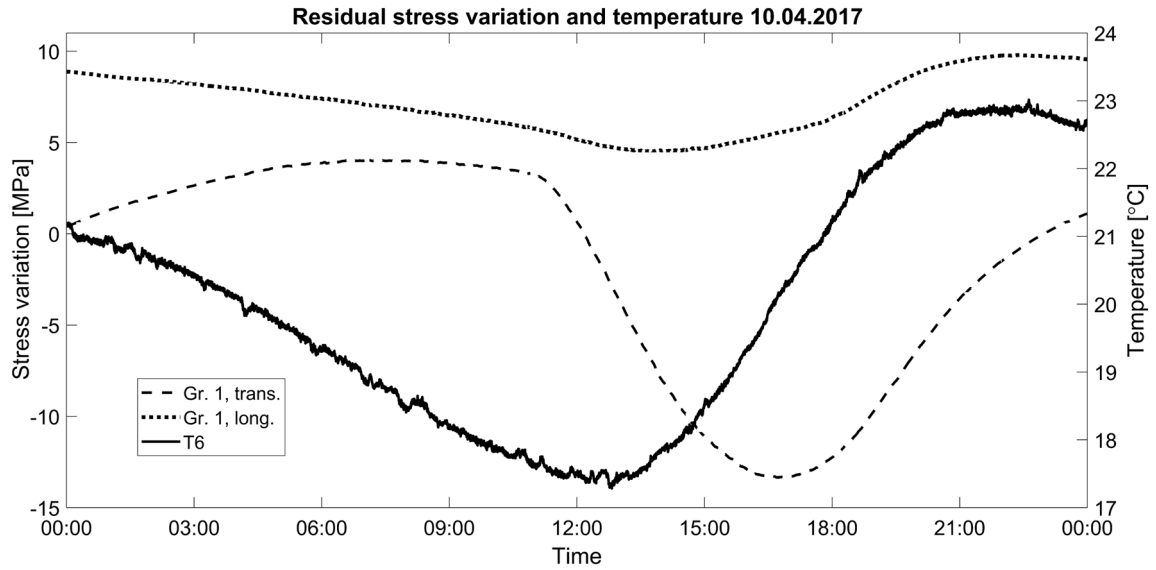

Fig. 8 Residual thermal stress variation and temperature recorded during 1 day

5 Measured stress ranges due to traffic and thermal actions

5.1 Histograms of stress ranges due to traffic and thermal actions

Figure 9a shows the histograms of stress ranges originating from temperature variation and Fig. 9b from traffic loading. The histograms were prepared for measurements between January 20, 2017 and April 10, 2019, thus 602 full days of data. Stress is determined by multiplying the strain readings with the modulus of elasticity of 205 GPa for steel rebars. Only the results from gauges of the transversal rebar from Group 1 and longitudinal rebar from Group 2 are shown. The other two gauges failed prematurely; however, their responses were similar to the presented ones.

The thermal stress range histograms were prepared by taking the thermal stress of each day and composing them together. Then, the rainflow counting algorithm was applied to these data. In this way, the day-to-day offsets are not considered, since the effect of windowing is avoided. The stress values due to traffic loading were treated separately, day after day.

Figure 9 reveals that, firstly, the maximum stress ranges due to both traffic and partially restrained thermal expansion are similar for the transversal rebar. The temperature-induced

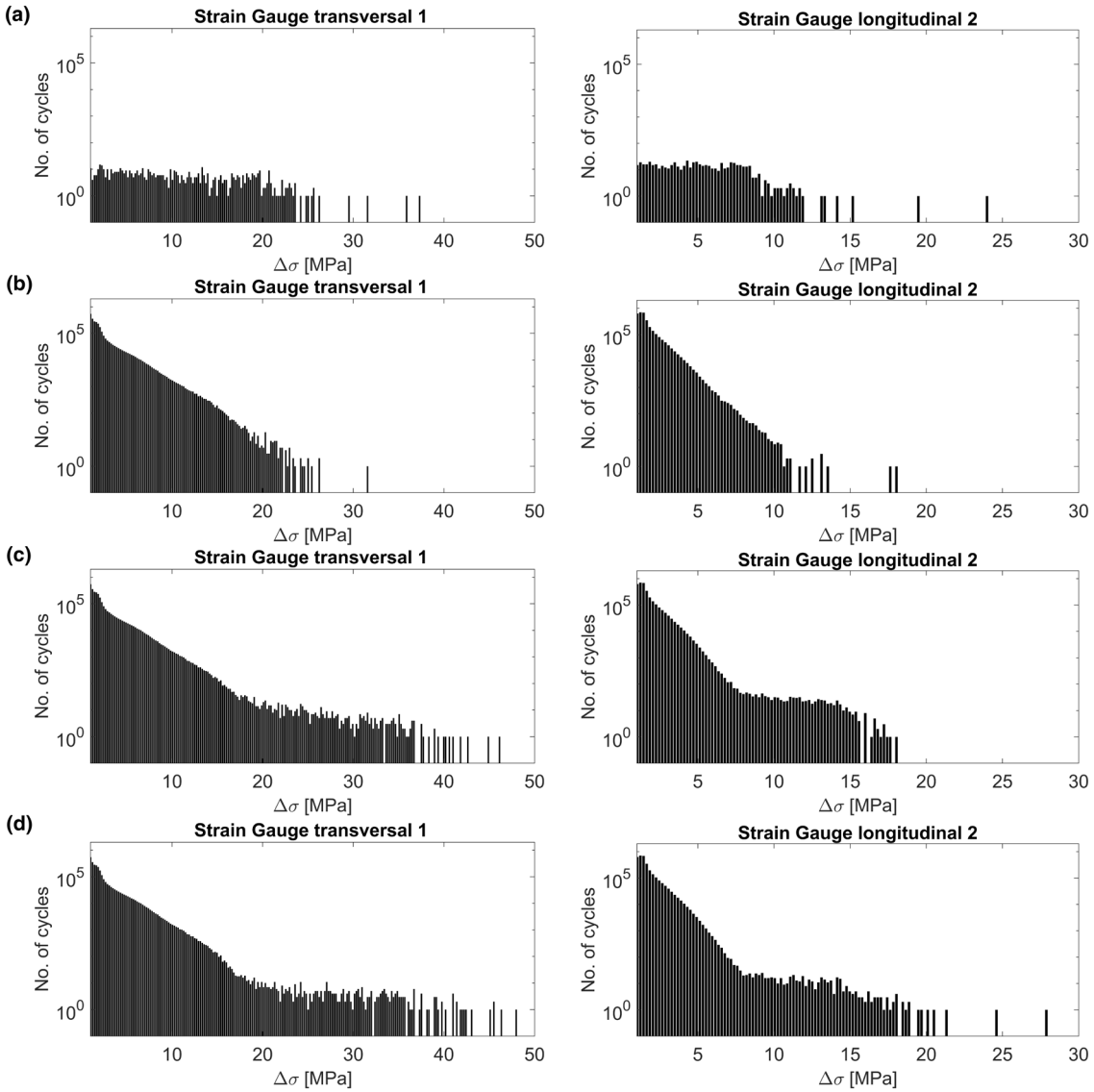

Fig. 9 Histograms of stress ranges induced by: **a** temperature (treated separately), **b** traffic (treated separately), **c** combined temperature and traffic with 24 h windowing and **d** combined temperature and traffic with 75 days windowing. These histograms are given for the whole monitoring period (602 days) and correspond to gauges: transversal from Group 1 and longitudinal from Group 2

stress ranges are even higher than traffic-induced stress ranges for the longitudinal rebar. Obviously, the number of cycles due to the traffic is much higher than that due to the temperature.

Secondly, the stress ranges in the steel rebars are far below the constant amplitude fatigue limit (CAFL) of 120 MPa according to the Swiss standard for existing structures SIA 269 [19]. Thus, and since the readings were taken in the determinant zone of the most likely highest stresses, the deck slab is not prone to fatigue damage.

5.2 Effect of windowing of the rainflow algorithm on stress range determination

As presented above, both thermal and traffic-induced stress cycles are fatigue relevant. However, the rainflow counting algorithm is sensitive to windowing, and the temperature and traffic-induced effects are therefore treated separately. For the sake of a sensitivity study, another procedure was followed as well.

First, the original signal was divided into as few windows as possible due to computational programme limits, i.e., eight windows of a size of 75 days. Then, since it is the negative of thermal stresses that is observed (Eq. (2)), the "thermal wave" was separated from the raw data as described previously, inverted and summed again with the traffic-induced strain readings. In this way, after multiplication with the modulus of elasticity, the complete stress range spectrum in rebar was obtained (Fig. 9d). To visualize the influence of windowing, the signal prepared in the same way but with the daily window is presented in Fig. 9c.

The effect of windowing is visible only in the highest values of stress range. This is due to the season-to-season thermal variations that are larger than the daily temperature variations. However, these cycles are rare and can be considered as irrelevant with respect to fatigue. Thus, a window length of 24 h for the rainflow counting should actually be used, as it is computationally much less expensive and sufficiently precise.

The 'tail' of histograms in Fig. 9c is longer than in Fig. 9b, representing the largest stress range values due to the temperature and heavy trucks combined. They occur when one truck is passing while the thermally induced stress cycle is close to minimum, and another truck is passing at the peak of the diurnal stress cycle. The difference between peaks of these events, thus the maximum stress cycle, cannot be captured by the traditional approach when temperature and traffic strains are separated. However, when the recorded stress range is far below the CAFL like in the present case, this difference is not relevant. On the contrary, when the stress range due to traffic is close or higher than the CAFL, the temperature effects should be taken into account, as they might be significant even for relatively simple structural elements. This is confirmed in Eurocode 2 [23] clause 2.3.1.2 stating that thermal effects should be taken into account in the analysis of fatigue limit state only if they are significant.

It should be noted that the variation of structural response due to change of temperature is inherently present in the traffic part of recorded stresses as described in chapter 6.

6 Theoretical fatigue damage

The Palgrem–Miner rule and fatigue resistance curve given in SIA 269/2 [19] were used for the calculation of traffic-induced apparent theoretical damage due to fatigue. The fatigue resistance of the present straight rebars is defined by a detailed category of 150 MPa at 2 million cycles; the slope in the S–N-diagram is 4 with a breakpoint at 5 million cycles and 120 MPa [24]. The damage should be called "apparent", as all the stress cycles are below the CAFL, and thus no real damage takes place. Damage accumulation was conducted here for the sake of comparison only, with a slope of 7 below the CAFL.

Figure 10 presents the daily apparent damage and mean temperature of the deck slab (thermocouple T6). The peaks of damage due to the isolated events are clearly visible.

The fluctuation of daily damage comes not only from traffic's stochastic nature, but also from the change of material and structural properties due to the temperature variation. At higher temperature, the contribution of the asphalt pavement is lower due to the lower stiffness [3, 13, 25]. Thus, the contribution of steel rebars is higher in response. This effect is visible in Fig. 10 as well. This proves also that the strain measurements were reliable.

7 Comparison of results from monitoring with calculations using a standardized load model

Since the deck slab of the box girder was originally relatively thin (18 cm), its fatigue performance was of concern before the strengthening with a UHPFRC layer. Below, a simplified fatigue analysis of the UHPFRC strengthened, 22 cm-thick deck slab in transversal direction is presented.

The deck slab (Fig. 11) can be represented simply by an elongated plate fixed along its longer sides. As the haunched parts are much stiffer than the slab itself, a span of 3 m is adopted for this calculation. A finite element model using shell elements was prepared to calculate the bending moments in the deck slab. The tandem axle loads of load model 1 according to European Standard [26] was applied to determine fatigue-relevant stress values in the

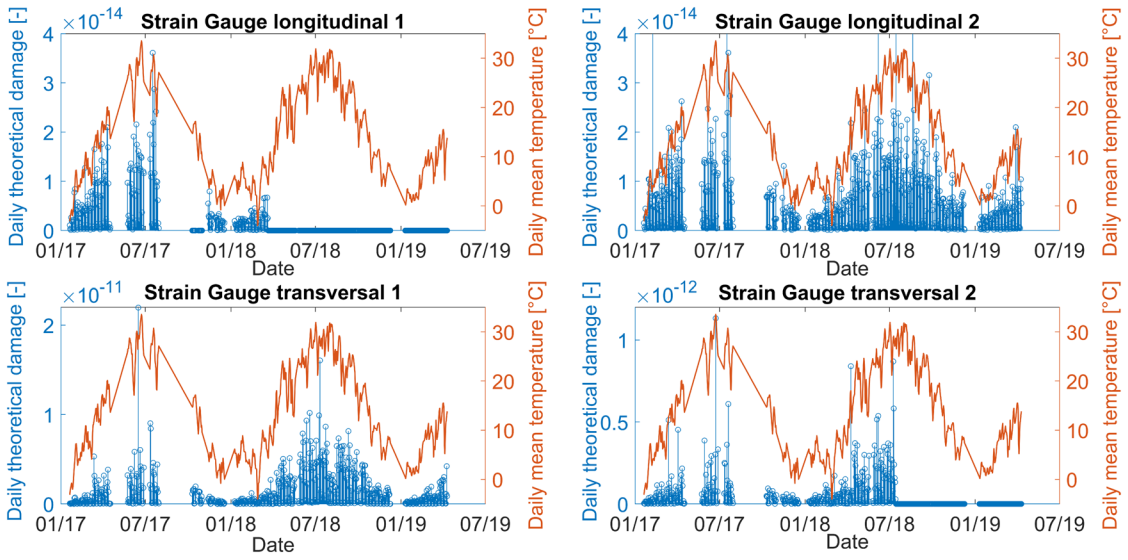

Fig. 10 Daily apparent damage and daily mean temperature of slab

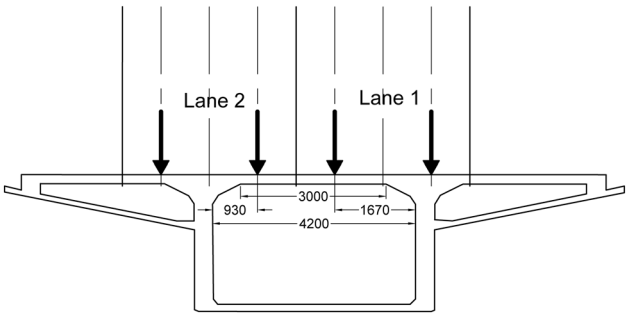

Fig. 11 Cross section of the superstructure with layout of the fatigue load model (dimensions in mm)

rebars. The tandem consists of two axles spaced by 1.2 m with characteristic axle load $Q_{k1} = 300$ kN.

According to the Swiss standard for existing structures [27], this axle load is updated to account for more realistic traffic loading:

$$Q_{fat} = Q_{k1} \cdot \alpha_{Q1,act} \cdot \gamma_{Ff} = 300\,\text{kN} \cdot 0.7 \cdot 1.0 = 210\,\text{kN}, \quad (3)$$

where Q_{k1} is the characteristic axle load on lane 1; $\alpha_{Q1,act}$ is the updating factor for road traffic; γ_{Ff} is the partial load factor for fatigue. The fatigue load model is positioned on the real, rightmost lane of traffic (Fig. 11) and the wheel force is distributed on the square area with an edge length of 0.4 m.

The calculated maximum positive bending moment is equal to 24 kNm, and the computed strain and stress distributions due to this moment are given in Table 1. The maximum stress range in the rebars is just below the CAFL. This is because the strengthening of the structure was designed using the method presented here.

Table 1 Calculated stress distribution in the deck slab under maximum positive bending moment 24 kNm/m

Layer	Strain [‰]	Stress [MPa]
UHPFRC	− 0.13	− 7
Reinforcement in UHPFRC	− 0.04	− 9
Concrete	N/A	N/A
Upper reinforcement in concrete	0.09	18.2
Lower reinforcement in concrete	0.53	108

N/A not applicable

Table 1 reveals that the calculated stress range using the code-based load model is about four times higher than the measured maximum stress range. This large difference comes, among others, from the consideration of a high dynamic amplification factor implicitly present in the code-based load model [28] leading to overestimating the load by a factor of almost two. Eventual dynamic effects on the stress in the rebar are actually implicitly included in the monitoring data that also show no notable dynamic response in the case of the present massive concrete structure. In fact, Fig. 3 shows that the passage of a vehicle axle does not produce any vibration of the deck slab, since the strain state returns immediately to the one before the passage. In addition, the static axle load considered in the code-based fatigue load model is higher than the measured mean static axle load using weigh-in-motion data from current vehicles in operation in Switzerland [29] and Europe.

Obviously, current methods of calculation of stresses in bridge elements lead to very conservative and thus

uneconomical results in the safety verification of existing bridges. Consequently, the method of direct measurement and monitoring of fatigue action effects on bridge elements should be deployed in case of fatigue concerns before any bridge intervention is undertaken.

8 Conclusions

This paper presents results from the 28-month-long monitoring of the reinforced concrete deck slab of a highway viaduct, which was strengthened with R-UHPFRC. This campaign was realized with thermocouples and strain gauges, glued directly to steel rebars. The structural response of the deck slab under both thermal and traffic-induced strains is discussed. The following conclusions can be drawn:

- In massive concrete bridge structures, stress ranges due to traffic loading and temperature action can be of similar magnitude.
- Stress variation due to the partially restrained thermal expansion is fatigue relevant when combined with high traffic-induced stress cycles. The two action effects should be treated together to identify relevant combinations.
- Windowing of 24 h using the rainflow counting algorithm is effective to gather thermally induced stress ranges with sufficient precision.
- The yearly and seasonal cycles of residual stresses due to restrained thermal expansion are not fatigue relevant, and thus do not need to be considered for fatigue safety verification.
- Fatigue-relevant stress ranges, as obtained from monitoring in the investigated deck slab portion of the viaduct, are significantly smaller than the CAFL of the determinant rebar.
- Measured stress values are significantly smaller than the corresponding stress values obtained from calculation using load models as defined in standards.

Acknowledgements This project has received funding from the European Union's Horizon 2020 research and innovation program under the Marie Skłodowska-Curie grant agreement No. 676139.

References

1. Nilimaa J, Bagge N, Häggström J, Blanksvärd T, Sas G, Täljsten B, Elfgren L (2016) More realistic codes for existing bridges. In: Challenges in design and construction of an innovative and sustainable built environment. Presented at the 19th IABSE Congress, Stockholm, p 9
2. Brühwiler E, Bastien-Masse M, Mühlberg H, Houriet B, Fleury B, Cuennet S, Schär P, Boudry F, Maurer M (2015) Strengthening the Chillon viaducts deck slabs with reinforced UHPFRC. In: IABSE Symposium Report. International Association for Bridge and Structural Engineering, pp 1–8
3. Martín-Sanz H, Avendano Valencia LD, Dertimanis V, Chatzi E, Brühwiler E (2018) Monitoring of Chillon viaduct after strengthening with UHPFRC. In: Proceedings, 9th International Conference on Bridge Maintenance, Safety and Management (IABMAS 2018), Melbourne, Australia. https://doi.org/10.3929/ethz-b-000316309
4. Denarié E (2005) SAMARIS D22—full scale application of UHPFRC for the rehabilitation of bridges—from the lab to the field (No. D22). In: EU 5th FWP SAMARIS project sustainable and advanced materials for road infrastructure WP 14: HPFRCC (high performance fibre reinforced cementitious composites) for rehabilitation deliverable D22. SAMARIS, Brussels, Belgium
5. Brühwiler E (2020) UHPFRC technology to enhance the performance of existing concrete bridges. Struct Infrastruct Eng 16:94–105. https://doi.org/10.1080/15732479.2019.1605395
6. SIA 2052 (2016) SIA 2052:2016 UHPFRC—materials, design and construction (in French and German)
7. Anderegg P, Brönnimann R, Meier U (2014) Reliability of long-term monitoring data. J Civ Struct Health Monit 4:69–75. https://doi.org/10.1007/s13349-013-0047-2
8. Frangopol DM, Alfred S, Sunyong K (2008) Bridge reliability assessment based on monitoring. J Bridge Eng 13:258–270. https://doi.org/10.1061/(ASCE)1084-0702(2008)13:3(258)
9. Leander J, Andersson A, Karoumi R (2010) Monitoring and enhanced fatigue evaluation of a steel railway bridge. Eng Struct 32:854–863. https://doi.org/10.1016/j.engstruct.2009.12.011
10. Li ZX, Chan THT, Ko JM (2001) Fatigue analysis and life prediction of bridges with structural health monitoring data—part I: methodology and strategy. Int J Fatigue 23:45–53. https://doi.org/10.1016/S0142-1123(00)00068-2
11. Sousa H, Costa BJA, Henriques AA, Bento J, Figueiras JA (2016) Assessment of traffic load events and structural effects on road bridges based on strain measurements. J Civ Eng Manag 22:457–469. https://doi.org/10.3846/13923730.2014.897991
12. Brownjohn JMW, Kripakaran P, Harvey B, Kromanis R, Jones P, Huseynov F (2016) Structural health monitoring of short to medium span bridges in the United Kingdom. Struct Monit Maint 3:259–276. https://doi.org/10.12989/smm.2016.3.3.259
13. Treacy MA, Brühwiler E (2015) Action effects in post-tensioned concrete box-girder bridges obtained from high-frequency monitoring. J Civ Struct Health Monit 5:11–28. https://doi.org/10.1007/s13349-014-0097-0
14. Massicotte B, Picard A (1994) Monitoring of a prestressed segmental box girder bridge during strengthening. PCI J 39:66–80
15. Chen C, Wang Z, Wang Y, Wang T, Luo Z (2017) Reliability assessment for PSC box-girder bridges based on SHM strain measurements. J Sens 2017:13. https://doi.org/10.1155/2017/8613659
16. Barr PJ, Stanton JF, Eberhard MO (2005) Effects of temperature variations on precast, prestressed concrete bridge

girders. J Bridge Eng 10:186–194. https://doi.org/10.1061/(ASCE)1084-0702(2005)10:2(186)
17. Herwig A (2008) Reinforced concrete bridges under increased railway traffic loads. École polytechnique fédérale de Lausanne, Thesis No 4010, Lausanne, Switzerland
18. Schläfli M (1999) Ermüdung von Brückenfahrbahnplatten aus Stahlbeton. École Polytechnique Federale de Lausanne, Thesis No 1998, Lausanne, Switzerland. https://doi.org/10.5075/epfl-thesis-1998
19. SIA 269/2 (2011) SIA 269/2:2011 Existing structures—concrete structures
20. Mallett GP (1991) Fatigue of reinforced concrete, state-of-the-art review. HMSO, London
21. Kromanis R, Kripakaran P (2016) SHM of bridges: characterising thermal response and detecting anomaly events using a temperature-based measurement interpretation approach. J Civ Struct Health Monit 6:237–254. https://doi.org/10.1007/s13349-016-0161-z
22. Hoffmann K (1974) Applying the Wheatstone bridge circuit (No. S1569-1.3 en). HBM
23. EC2 (2005) EN-1992-1-1: Eurocode 2: design of concrete structures—part 1–1: general rules and rules for buildings
24. SIA 262 (2003) SIA 262:2003 concrete structures
25. Favre R, Hassan M, Burdet O (1994) Statistical data combined with linear and non-linear analysis to interpret bridge load tests. In: 4th Int. Conf. Short Medium Span Bridg, pp 1197–1208
26. EC1 (2003) EN 1991-2: Eurocode 1: actions on structures—part 2: traffic loads on bridges
27. SIA 269/1 (2011) SIA 269/1:2011 existing structures—actions
28. Ludescher H, Brühwiler E (2009) Dynamic amplification of traffic loads on road bridges. Struct Eng Int 19:190–197. https://doi.org/10.2749/101686609788220231
29. Statistical Annual Reports of Swiss Federal Road Office (ASTRA) on weight in motion results for years 2003–2011. https://www.astra.admin.ch/astra/de/home/dokumentation/verkehrsdaten/daten-publikationen/gewichtserfassung.html (in German). Accessed 18 Oct 2019